

EXPERIMENTAL INVESTIGATION AND OPTIMIZATION OF PERMANENT MAGNET MOTOR BASED ON COUPLING BOUNDARY ELEMENT METHOD WITH PERMEANCES NETWORK

S. Touati

Nuclear Research Centre of BIRINE
Bp 180, Ain Oussera 17200, Algeria

R. Ibtiouen and O. Touhami

Ecole Nationale Polytechnique d'Alger (ENP)
El-Harrach DZ-16200, Algeria

A. Djerdir

FCLab, SET UTBM
13 rue Thierry Mieg, Belfort 90000, France

Abstract—In the first part of this work, we develop a model to compute linkage fields in Outer Rotor Permanent Magnets synchronous machines (OR-PMSM), a structure which is often used in the automotive traction motors. To carry out such a design, we usually employ Finite Element analysis (FEA) software even if it is time consuming. Other designers prefer the Permeances Network Method (PNM) which is less accurate and needs offline FEM results to evaluate the unknown air-gap permeances. Comparatively, between FEM and BEM, the first method is more precise whereas the second is faster in computing times. We propose here a new technique using the hybridization of both methods in order to gain the advantages of the two techniques, i.e., a relatively accurate and fast methods, so the high ratio of fast running to computing errors has been achieved. The second part deals with the multi-objective design optimization of the studied motor. To do this, we choose the decrease of cogging torque and the increase of torque as objectives applied to multi-objective optimization (MO) process.

1. INTRODUCTION

Generally, a designer can use different kinds of models in order to size and optimize a device. These models, as finite-element model or boundary element method, can be very precise, but need much computation time, limiting the number of parameters and constraints that can be taken into account [1]. So the designer should also use, especially in the first step of the design, when it is necessary to size a large number of parameters with many constraints, a more macroscopic approach as the permeances network approach [1, 2]. In spite of its short simulation time, the latter has not largely been used because of its bad accuracy and the difficulties to implement: as soon as the designer has built a network topology, complicated tasks have to be done as generating the equations and solving them, especially when saturating materials are used [3, 4]. This paper describes a new approach based on the coupling of BEM and PNM for the performance analysis of the studied machine. Indeed, in order to increase the accuracy of the equivalent Permeance Network modeling of the studied machine, the BEM is used to calculate the air-gap permeances [2, 5]. The originality of this work is to make a global analysis of the OR-PMSM only with a permeances network method without the need for other additional softwares to calculate permeances in the air-gap, which allows to reduce overall calculation time [6]. This hybrid method could then be coupled with other algorithms of optimal design, control and diagnostics in real time drive operations. On the base of this method, a software tool has been developed for PMSM modeling, and it has been successfully applied to a reversed structure PMSM dedicated to an automotive application. An example of this structure is shown in Figure 1.

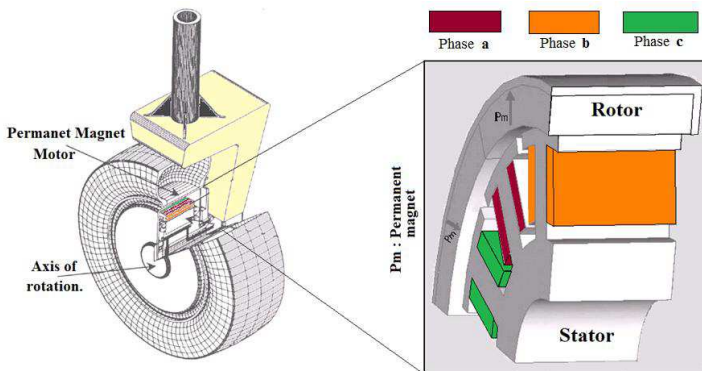


Figure 1. Application principale for the studied motor.

2. STRUCTURE OF OUT-ROTOR PERMANENT MAGNET MOTOR

Studied machine is available at the SET-UTBM laboratory, and it is integrated in a bicycle wheel engine-wheel as showed in Figure 2. This machine is an exterior-rotor motor with 6 poles, 36 teeth and 3 phases full bridge circuit. For reasons of symmetry and by neglecting the extremity effects, one pole pair of the geometry is sufficient to model the entire machine as shown in Figure 3.

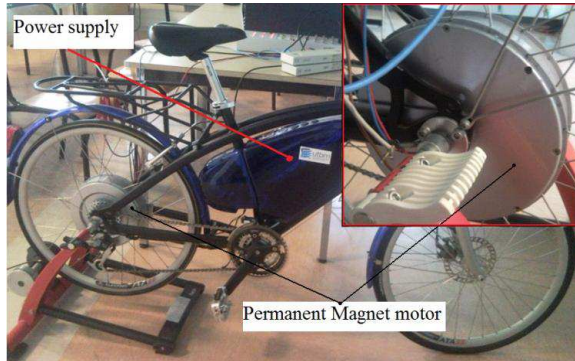


Figure 2. Set up of the studied machine in a bicycle wheel.

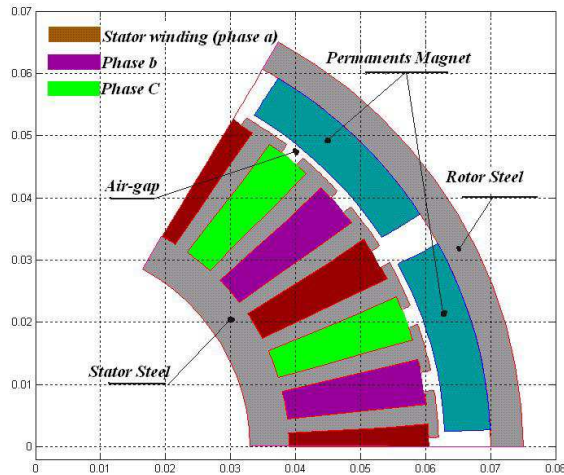


Figure 3. Two dimensional transverse cross section of the studied motor.

3. APPLICATION OF BOUNDARY INTEGRAL METHOD

In this section, a two-dimensional (2D) boundary-element method coupling, based on A - ϕ formulation was developed, from Maxwell equations in the limit of stationary field, taking into account the constitutive relationships [7, 8]:

$$H = f(B), \quad J = \sigma \cdot E \quad (1)$$

Using Coulomb gauge $\nabla \cdot A = 0$, the two-dimensional governing equation for the studied machine is expressed in magnetic vector potential by the following:

$$\nabla \cdot A = -\mu_0 \cdot J_S \quad (2)$$

where

A : Component of magnetic vector potential

J_0 : Current density

The field sources are the impressed current sources J_0 in the air and the equivalent current density result from magnetization of permanent magnets.

3.1. Setting of the Integral Equations

We define a function G such:

$$\nabla^2 G \cdot \delta(r) = 0 \quad \nabla^2 G = -\delta(r) \quad (3)$$

The solution of this equation gives the second identity of Green which is represented by:

$$G(P, Q) = -\frac{1}{2 \cdot \pi} \ln(r_{PQ}) \quad (4)$$

The function $G(P, Q)$ corresponds to the potential created by a source at the point Q . However, the derivation is carried out at point P (Figure 4). This function depends only on the distance $r_{PQ} = |PQ|$.

The multiplication of the two members of Equation (2) by the function of Green G gives:

$$G \cdot \nabla^2 \cdot A = -\mu_0 \cdot J_S \cdot G \quad (5)$$

The multiplication of the two members of the equation of Green (3) by the magnetic potential vector A gives:

$$-A \cdot \nabla^2 \cdot G = -A \cdot \delta(r) \quad (6)$$

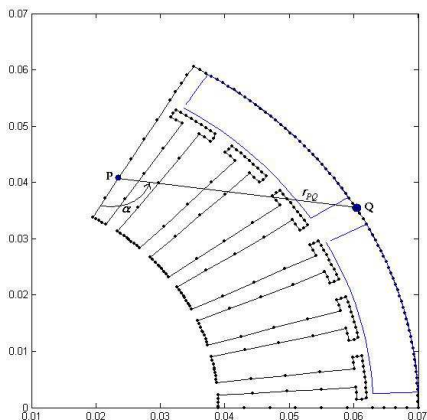


Figure 4. Contour of the equivalent studied domain.

The member with member addition of these two last relations (5) and (6) gives the following result:

$$G \cdot \nabla^2 \cdot A - A \cdot \nabla^2 \cdot G = A \cdot \delta(r) - \mu_0 \cdot J_S \cdot G \quad (7)$$

The integration of this last result on the domain non saturable D gives the relation:

$$\oint_D (G \cdot \nabla^2 \cdot A - A \cdot \nabla^2 \cdot G) \cdot d\Omega = A_l - \oint_D (\mu_0 \cdot J_S \cdot G) d\Omega \quad (8)$$

$$\oint_D (G \cdot \nabla^2 \cdot A - A \cdot \nabla^2 \cdot G) \cdot d\Omega = \oint_D (A \cdot \delta(r) - \mu_0 \cdot J_S \cdot G) d\Omega \quad (9)$$

The first member of the integral Equation (9) can be brought back to an integral on the contour of the field, by using the identity of Green:

$$\oint_{\Gamma} \left(G \cdot \frac{\partial A}{\partial n} - A \cdot \frac{\partial G}{\partial n} \right) \cdot d\Gamma = C_l A_l - \int_D \mu_0 \cdot J_S \cdot G d\Omega \quad (10)$$

using Gauss method integration, the last equation can be written in the following matrix form:

$$C_i \cdot A_i + B_i + \sum_{j=1}^n H_{ij} \cdot A_j = \sum_{i=1}^n G_{ij} \cdot \frac{\partial A_j}{\partial n} \quad (11)$$

where $c_i = \frac{\alpha}{2\pi}$, α is defined in Figure 4

$$B_i = \iint_{\Omega} G \cdot J_{ex} \cdot ds, \quad H_{ij} = \int_{l_f} \frac{\partial G}{\partial n} \quad \text{and} \quad G_{ij} = \int_{l_f} G \cdot dl \quad (12)$$

Introducing boundary conditions and arranging the previous Equation (6), we obtain a final matrix equation to resolve:

$$[S] \cdot [A] = [F] \quad (13)$$

3.2. Air-gap Permeance Computation

The information of potential vector is then exploited to calculate the air-gap permeances taking into account stator slot openings:

$$P_{ag} = \frac{(A_2 - A_1) \cdot l}{B \cdot S} \quad (14)$$

l is the longitudinal length of our structure; A_1 and A_2 are respectively the potential in the extrimities of the stator slot; and S is the surface of the slot on the air-gap.

The permeances in the air-gap are computed by means of Equation (14) using the boundary element method. Figure 5 represents the comparison between the permeance obtained by an free finite element method software (FEMM) and the other obtained by our developed boundary element method. This figure shows an acceptable concordance between the two methods.

3.3. Constant Permeance Computation

At this level, we compute the constant permeances related to different parts of the machine whose geometry remains unchanged whatever the rotor position. The permeances of stator and rotor steels as well as of the permanent magnet are defined by a cylindrical portion having a length l (length of machine), an opening angle α , and a thickness

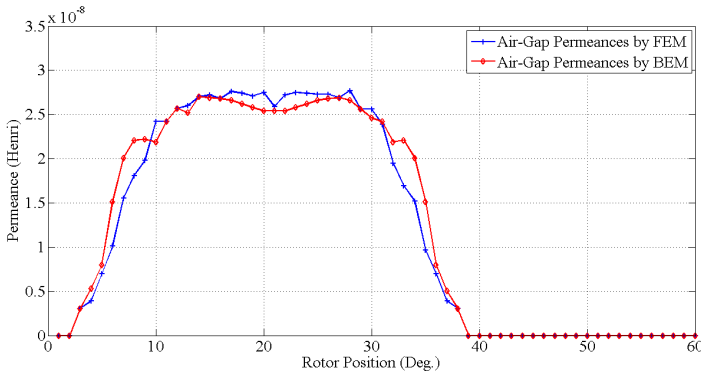


Figure 5. Permeance variation in the air-gap vs rhe rotor position.

defined by internal and external radii, namely r_{int} and r_{ext} . The most complicated task is building the topology of the network. Its knowledge can be obtained from FEM simulations, in order to understand how the flux propagates in the motor as shown in Figure 6.

Thus stator and rotor permeances ($P_{r,s}$) and the permanent magnet ones (P_{pm}) are expressed as follows [3, 4]:

$$P_{r,s} = \mu_0 \mu_r \cdot s \cdot \frac{l \cdot \ln \cdot \left(\frac{r_{ext}}{r_{int}} \right)}{\alpha}, \quad P_{pm} = \mu_0 \mu_{pm} \cdot \frac{\alpha}{\ln \cdot \left(\frac{r_{ext}}{r_{int}} \right)} \quad (15)$$

After applying these expressions to the studied motor, we obtain the constant permeances which correspond to the principle flux paths observed through a FEM simulation of motor in the no-load state. Table 1 gives their values and locations inside the machine.

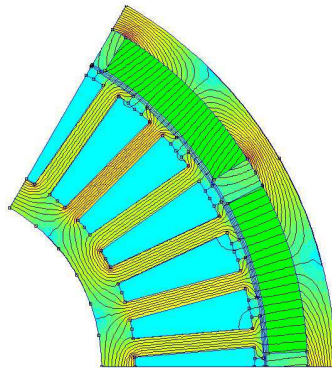


Figure 6. Flux lines in the studied motor by FEMM software.

Table 1. Constant permeances of the studied motor.

Permeance index	Location in the motor	Value (H)
P_r	Rotor steel permeance	$4.3286 \cdot 10^{-6}$
P_{pm}	Permanent magnet (PM) permeance	$2.8611 \cdot 10^{-7}$
P_{pm-pm}	Leakage permeance between PM poles	$8.26 \cdot 10^{-8}$
P_{st-st}	Leakage permeance between stator teeth	$3.6391 \cdot 10^{-8}$
P_{st}	Permeance of one stator teeth	$1.659 \cdot 10^{-4}$
P_S	Stator steel permeance	$1.1205 \cdot 10^{-4}$

3.4. Coupled PNM-BEM Modeling

The algorithm and equivalent network followed to achieve this operation is shown in Figure 7 and Figure 8 respectively.

The air-gap permeance is computed by including a magnetic field computation in that region through the BEM and starting from the geometry and materials characteristics for the studied machine. F_d is the magnetomotive force (MMF) of a stator teeth considering the magnetic reaction of stator currents, and F_a is the MMF of the north pole magnet.

In a way similar to electric circuits, a magnetic circuit or a network of permeances can be seen as a group of magnetic branches. In a permeance network, a magnetic teeth is composed of a permeance, in series with a MMF of teeth. The latter may easily be calculated using a linear combination of the various MMF of slots. The other magnetic branches consist of simple permeances containing a possible source of MMF mounted in series which could be of a permanent magnet. In

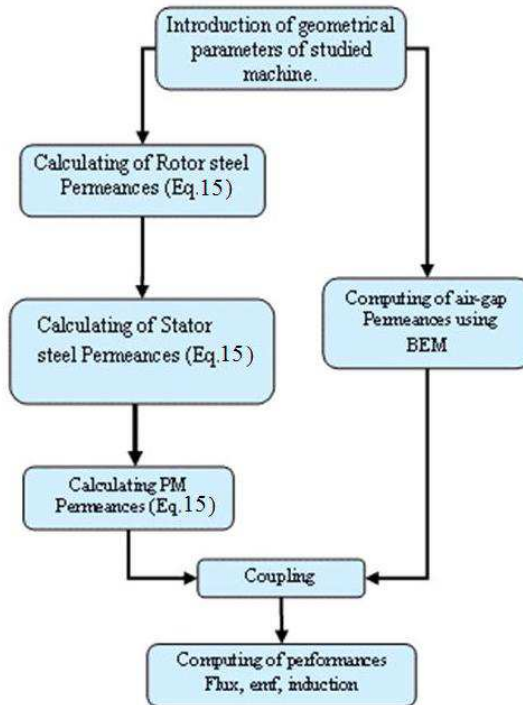


Figure 7. Flowchart of optimization process.

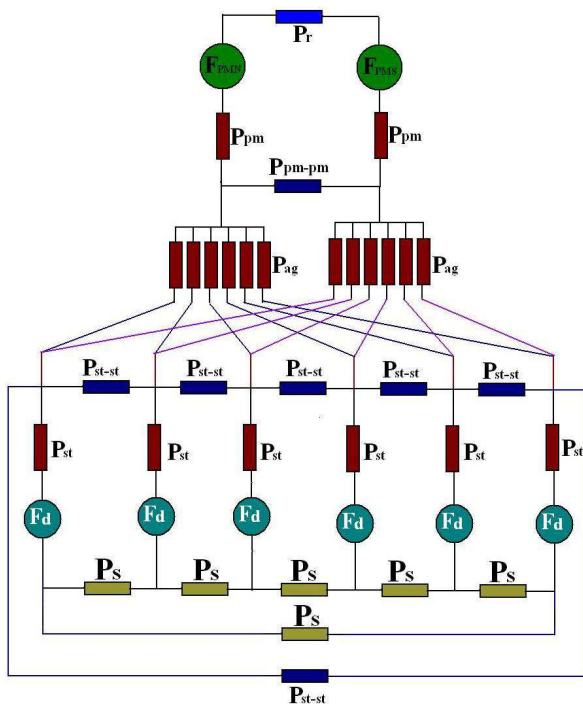


Figure 8. Equivalent permeance network.

a complete network of permeances, one must compute all the branch flux values and all the node magnetic potentials. For each magnetic tooth, we obtain the relation:

$$U_{dj} - U_{aj} = Fd_j + \frac{\phi_j}{P_j} \tag{16}$$

for the permanent magnets we have:

$$U_{dj} - U_{aj} = Fa_j + \frac{\phi_j}{P_j} \tag{17}$$

and for the a magnetic branch we have:

$$U_{dj} - U_{aj} = \frac{\phi_j}{P_j} \tag{18}$$

When scanning all the nodes of the circuit, we obtain a matrix relationship between the MMFs of different branches $[F]$, the magnetic potentials of different nodes $[U]$, and the permeance matrix $[G]$. So, for

a given stator windings current we can compute by a simple inversion, all the magnetic node potentials $[U]$ and thus air-gap flux density, EMFs, and electromagnetic torque of the machine.

3.5. Flux Linkage, EMF and Torque

The reluctance network model of the studied permanent magnet synchronous motor can be computed for any relative position of the rotor and stator. This allows a time stepping simulation in steady state operation. The motor is fed by trapezoidal three phase currents [9, 10]. The reluctance network model is then fed by the real instantaneous MMF. At each time step, the rotor is rotated by the corresponding angular step (1), the phase currents are updated, and the airgap permeance using boundary integral method is recomputed [11]. After each time step, the fluxes flowing through the teeth of the stator are available. From these fluxes and the average values of the vector potential at each stator slot, we can use the following relations [12]:

$$[A_{int}] = [ones] - [Tr_{inf}] * [\phi_{teeth}] \quad (19)$$

$$[A_{slot}] = [A_{int}] - \frac{1}{2} (\max([A_{int}]) + \min([A_{int}])) \quad (20)$$

where the matrix $[Tr_{inf}]$ and the vector $[ones]$ are given by:

$$[Tr_{inf}] = \begin{bmatrix} 1 & 0 & \dots & 0 \\ 1 & 1 & \dots & 0 \\ \cdot & \cdot & \dots & 0 \\ 1 & 1 & \dots & 1 \end{bmatrix} \quad \text{and} \quad [Ones] = \begin{bmatrix} 1 \\ 1 \\ \cdot \\ 1 \end{bmatrix} \quad (21)$$

with $N_S = 3 \cdot p \cdot q$ is the number of slots.

Knowing the average vector potential at each slot and the winding pattern, we can compute the flux linkage of each phase.

$$[\Psi_{ABC}] = n_{trn} \cdot [M_{wind}] * [A_{slot}] \quad (22)$$

After every electrical cycle, the flux linkage of each phase is available as a function of time. Numerical derivations using spline interpolation lead to the EMF waveforms [13].

$$[e_{ABC}] = \frac{d}{dt} \cdot [\Psi_{ABC}] \quad (23)$$

The mean value of the torque is computed by

$$T_{mean} = \frac{1}{\Omega \cdot T} \cdot \int_T (e_A \cdot i_A + e_B \cdot i_B + e_C \cdot i_C) \quad (24)$$

3.6. Experimental Validation

In the precedent section, we have developed a hybrid method, using permeances network as a main method and the boundary element method to evaluate permeances of the air-gap. To validate this method, we have mounted a set-up of the studied motor to acquire different measures as electromotive forces, currents and torque of the motor, as shown in the Figure 9.

Figure 10 shows the EMF of the first phase of the studied motor (the EMFs of the two other phases have the same waveforms but they are out of phase with an angle of regarding to the first one). It is seen that the obtained results from Boundary Element modeling have an acceptable agreement compared with the measured ones.

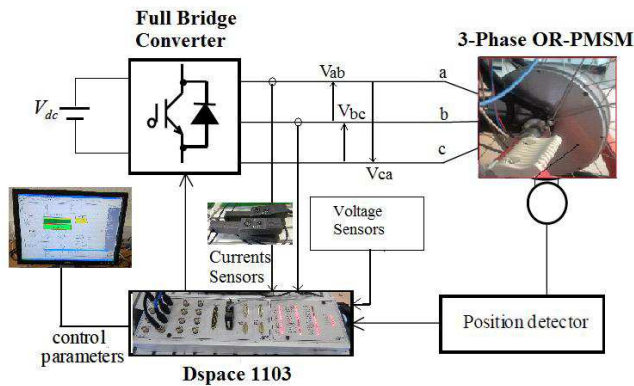


Figure 9. Diagram controls of the experimental tests.

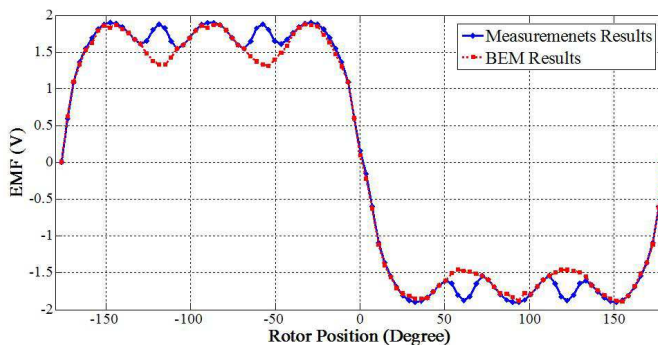


Figure 10. EMF waveform of the motor versus the rotor position.

Waveforms of the current in the stator winding are also represented in Figure 11. They are obtained by exploiting the machine in generate mode feeding a symmetrical triphase resistive load, of $100\ \Omega$ each one.

In Figure 12, we compare the dynamic electromagnetic torque developed by our model, with the indirectly measured torque. Indeed, starting from the measured currents and of the EMF, we use Equation (24) to deduce this torque. Figure 13 represents the magnetic potential vector in the air-gap obtained both by the method suggested and the finite element method. Whereas, Figure 14 represents the distribution of radial flux density in the air-gap obtained by the two methods.

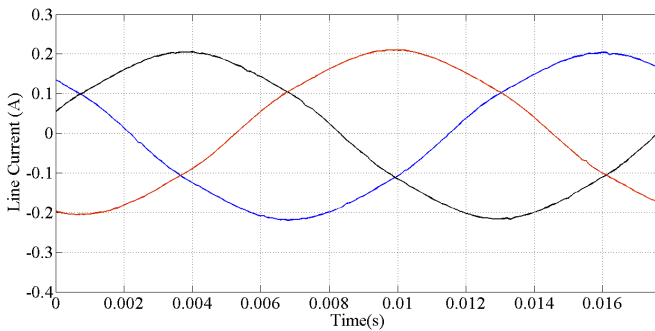


Figure 11. Measured current waveforms delivered by the machine in generate mode.

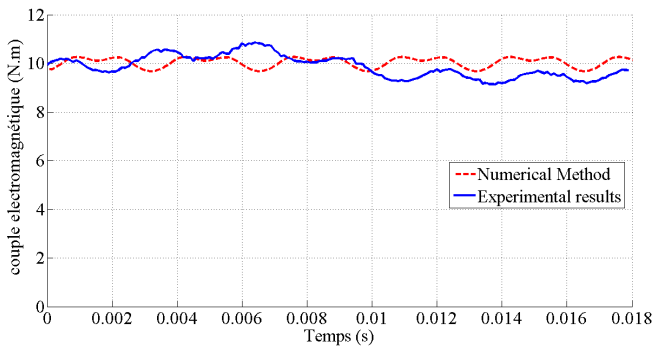


Figure 12. Dynamic electromagnetic torque.

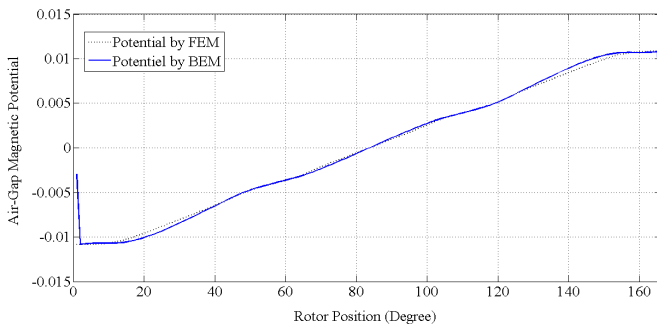


Figure 13. Air gap potential vector.

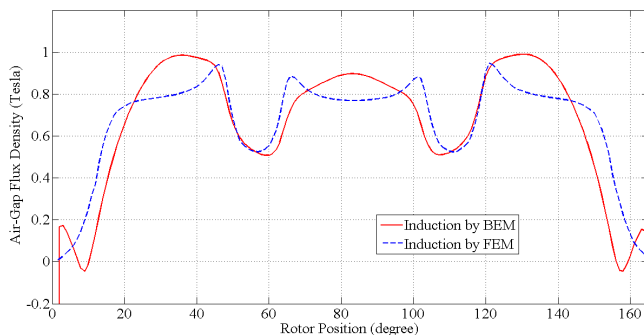


Figure 14. Air-gap flux density.

4. MULTIOBJECTIVE OPTIMIZATION DESIGN USING GENETIC ALGORITHM

4.1. Multiobjective Optimization Problem

In most cases, a general multi-objective problem can be described as follows [14, 15]:

The design parameters: $\vec{x} = [x_1, x_2, \dots, x_D]$, $\vec{x} \in R^D$.

The design parameters: $F = \{g_j(\vec{x}) \leq 0, j = 1, \dots, m\}$.

The boundary of the parameters: $x_i^L \leq x_i \leq x_i, i = 1, \dots, D$.

And the objective function set: $f(\vec{x}) = [f_1(\vec{x}), f_2(\vec{x}), \dots, f_k(\vec{x})]$.

where $f(x)$ is objective function, and x is called the decision vector belongs to the feasible region F formed by constraints $G(x)$. In general, there is a trade off relationship among the objective functions,

and it is difficult to minimize the objectives simultaneously [16–18]. The solution of MO problem is not a single point, but a family of nondominated points known as the PO solutions. Accordingly, the goal of MO problem is to find many different PO solutions as possible considering a MO problem. The Pareto optimality concept means that any two solutions x_1 and x_2 can have one of two possibilities: one dominates the other, or none dominates the other. In a minimization problem, a solution x_1 dominates x_2 if and only if the following conditions are satisfied [19]:

$$f_i(x_1) \leq f_i(x_2) (\forall i = 1, \dots, p) \quad (25)$$

In a maximization problem, a solution x_1 dominates x_2 which means that:

$$f_i(x_1) \geq f_i(x_2) (\forall i = 1, \dots, p) \quad (26)$$

4.2. Optimization of the Studied Motor

We use Genetic Algorithm to solve the multi-objective problem. This technique imitates the process of genetic evolution and natural

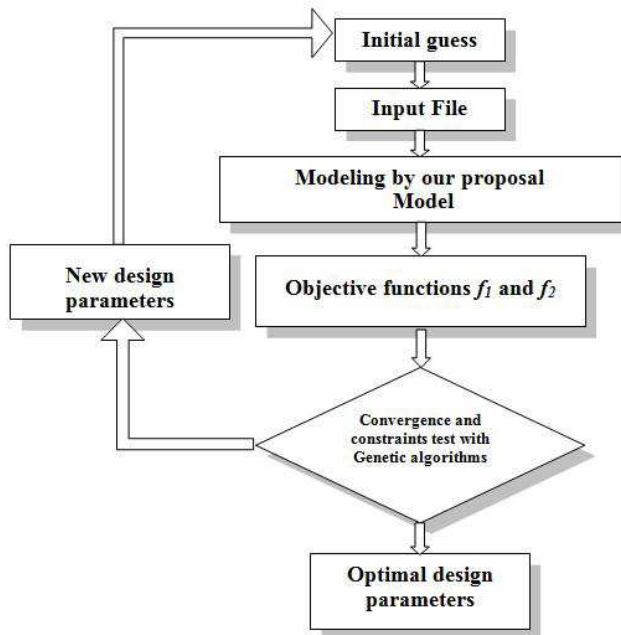


Figure 15. Flowchart of optimization process.

selection. It is considered one of the stochastic searching algorithms. Figure 15 shows the adopted flowchart of our optimisation process. Compared to conventional optimization algorithms, GA copes well with complex problems involving features such as multimodality, discontinuities, and disjoint feasible spaces. The objectives functions are selected to be the decrease of cogging torque and the increase of torque. The airgap length, teeth width and dead zone angle of PM are also selected as the design variables respectively. Those functions are defined as follows:

$$f_1(x) = \frac{(\Gamma_{\max} - \Gamma_{\min})}{\Gamma_{means}} \tag{27}$$

$$f_2(x) = \Gamma_{means} \tag{28}$$

where Γ_{\max} , Γ_{\min} and Γ_{means} are the maximum, minimal and means instantaneous torque respectively.

4.3. Optimisation Results and Discussion

A computer program using the MATLAB software was developed and has given the results below. The parameters of GA used for the design optimization were: The total number of the solutions is 250. As shown in Figure 16, it is known that there is trade off relationship between objectives, and the total interactive tendency in the objective domain can be grasped easily. The arrow points to the balanced final optimal solution selected from the PO solutions.

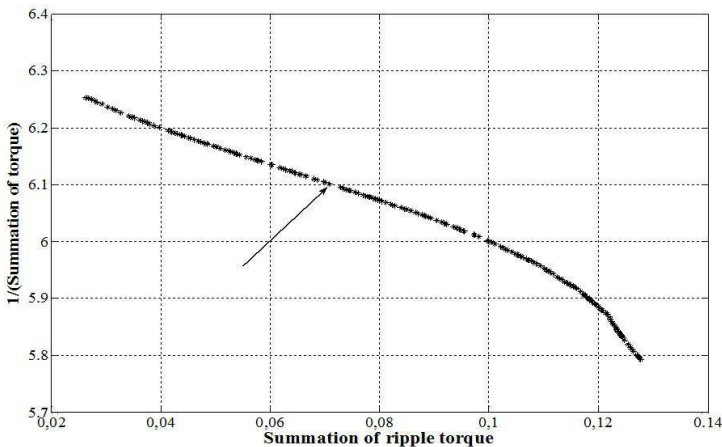


Figure 16. Pareto optimal solution for multiobjective design problem of BLDCM.

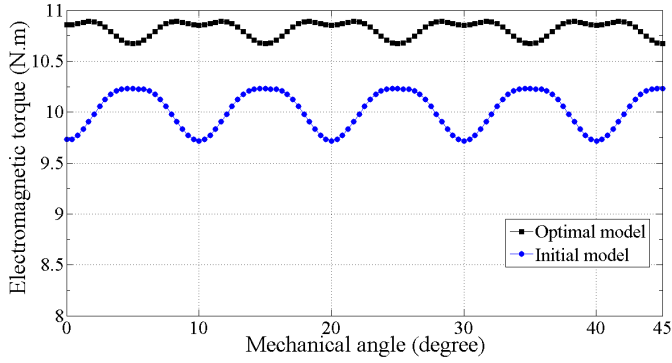


Figure 17. Comparison of torque simulated results between initial model and optimal model.

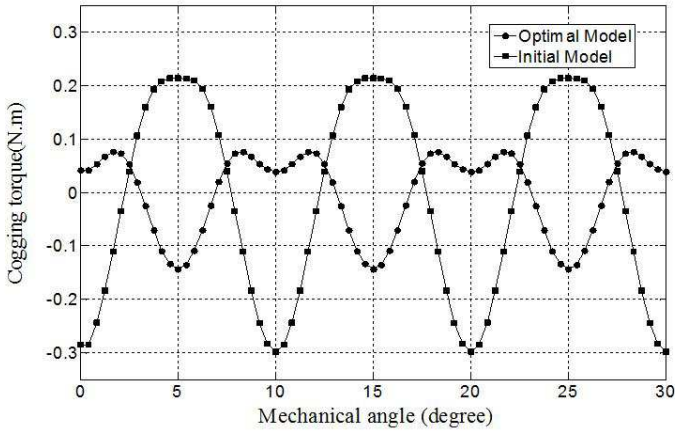


Figure 18. Comparison of cogging torque simulated results between initial model and optimal model.

Table 2. The constraints, initials and optimal variables values.

Design Variables	Constraints	Initial value	optimal value
Teeth width T_w	$2 \leq l_a \leq 5$	2	3.5 [mm]
Magnetic thickness	$5 \leq l_a \leq 10$	5	7 [mm]
Air-gap Length l_a	$0.25 \leq l_a \leq 1.0$	0.3	0.8 [mm]

The constraints, initial and optimal values in the design variables are given in Table 2. Figures 17 and 18 show the analysis results of cogging torque and torque characteristics comparing the initial model with the optimized model respectively. Compared to the initial model, the average torque is decreased by only 2.6.

5. CONCLUSION

The computed results, compared with those resulting from the code calculation flux 2D, show that the proposed method, based on coupling BEM with PNM, gives acceptable results to describe the magnetic behavior of the studied machine. The difference observed in Figure 7 can be due to not taking into account the saturation effect. The main advantage of this proposed technique is its simplicity and its fast execution time compared to the FEM method. The multi-objective optimization based on genetic algorithms and 2D Boundary Element Method was applied to the practical investigation of an optimal design of the permanent magnets synchronous motor built-in in a vehicle wheel. Indeed, starting from an initial model and using genetic algorithms, we have improved the performance of the structure taking into account the objective chosen. This method has the characteristic of being fast, relatively if we use the finite element method, which favors its use for not only design issues but also for solving problem inverses in electrical machines, especially the demagnetization problem.

APPENDIX A. MACHINE PARAMETERS

The main geometrical parameters of the studied structure are described in the following table:

Air-gap	Thickness	ent	1 mm
Definition of the magnets	Moderate material	Nd Fe B	-
	External diameter	R_r	140 mm
	Interior diameter	R_a	126 mm
	Thickness	h_a	7 mm
	Angular opening relating to a pole	t_a	85% of pole
Definition of the rotor	External diameter	R_{ext}	150 mm
	Interior diameter	R_r	142 mm
	Thickness	h_{cr}	5 mm

Definition of the stator	External diameter	R_s	124 mm
	Interior diameter	R_{int}	66 mm
	Height of the isthmus of tooth	h_{is}	1.5 mm
	Width of the isthmus of tooth	L_{is}	2.05 mm
	Width of a tooth r	l_d	3.4 mm
	height of a tooth	h_d	21.5 mm
	Height of the stator cylinder head	h_{cs}	6 mm
	Number of pair of poles	p	142 mm
	Numbers of slot by pole and phase	q	142 mm
	Length of iron	L_{fer}	142 mm

REFERENCES

1. Fredkin, R. and T. R. Koehler, "Hybrid method for computing demagnetizing fields," *IEEE Transactions on Magnetism*, Vol. 34, No. 10, 1064–1076, 1986.
2. Bettini, P., E. Brusa, M. Munteanu, R. Specogna, and F. Trevisan, "Static behavior prediction of microelectrostatic actuators by discrete geometric approaches," *IEEE Transactions on Magnetism*, Vol. 44, No. 6, 1606–1609, 2008.
3. Farooq, J., S. Srairi, A. Djerdir, and A. Miraoui, "Use of permeance network method in the demagnetization phenomenon modeling in a permanent magnet motor," *IEEE Transactions on Magnetism*, Vol. 42, No. 4, 2006.
4. Aiello, G., S. Alfonzetti, E. Diletto, and N. Salerno, "An iterative solution to FEM-BEM algebraic systems for open-boundary electrostatic problems," *IEEE Transactions on Magnetism*, Vol. 43, No. 4, 1249–1252, 2007.
5. Roisse, H., "Contribution la modlisation des systmes lectrotechniques par la mthode des rseaux de permance couples," Ph.D. Dissertation, Univ. Lille, France, 1998.
6. Perho, J., "Reluctance network for analysing induction machines," Ph.D. Dissertation, Helsinki Univ. Technology, Helsinki, Finland, 2002.
7. Vaseghi, B., N. Takorabet, and F. Meibody-Tabar, "Transient finite element analysis of induction machines with stator winding

- turn fault,” *Progress In Electromagnetics Research*, Vol. 95, 1–18, 2009.
8. Petrichenko, D., M. Hecquet, P. Brochet, V. Kuznetsov, and D. Laloy, “Design and simulation of turbo-alternators using a coupled permeance network model,” *IEEE Transactions on Magnetics*, Vol. 42, No. 4, 1259–1262, 2006.
 9. Jian, L. and K.-T. Chau, “Analytical calculation of magnetic field distribution in coaxial magnetic gears,” *Progress In Electromagnetics Research*, Vol. 92, 1–16, 2009.
 10. Priede, J. and G. Gerbeth, “Boundary-integral method for calculating poloidal axisymmetric AC magnetic fields,” *IEEE Transactions on Magnetics*, Vol. 42, No. 211, February 2006.
 11. Faiz, J. and B. M. Ebrahimir, “Mixed fault diagnosis in three-phase squirrel-cage induction motor using analysis of air-gap magnetic field,” *Progress In Electromagnetics Research*, Vol. 64, 239–255, 2006.
 12. Wu, K. L., G. Y. Delisle, D. G. Fang, and M. Lecours, “Coupled finite element and boundary element methods in electromagnetic scattering,” *Progress In Electromagnetics Research*, Vol. 2, 113–132, 1990.
 13. Botha, M. M. and J.-M. Jin, “On the variational formulation of hybrid finite element-boundary integral techniques for electromagnetic analysis,” *IEEE Transactions on Antennas Propag.*, Vol. 52, No. 11, 3037–3047, November 2003.
 14. Trlep, M., L. Skerget, B. Kreca, and B. Hribernjak, “Hybrid finite element — Boundary element method for nonlinear electromagnetic problems,” *IEEE Transactions on Magnetics*, Vol. 31, No. 3, 1380–1383, 1995.
 15. Fetzer, J., S. Kurz, G. Lehner, and W. M. Rucker, “Application of BEM-FEM coupling and the vector Preisach model for the calculation of 3D magnetic fields in media with hysteresis,” *IEEE Transactions on Magnetics*, Vol. 36, No. 4, 1258–1262, July 2000.
 16. Hua, Y., Q. Z. Liu, Y. L. Zou, and L. Sun, “A hybrid FE-BI method for electromagnetic scattering from dielectric bodies partially covered by conductors,” *Journal of Electromagnetic Waves and Applications*, Vol. 22, No. 2–3, 423–430, 2008.
 17. Chen, J. and Q. H. Liu, “A non-spurious vector spectral element method for Maxwell’s equations,” *Progress In Electromagnetics Research*, Vol. 96, 205–215, 2009.
 18. Ravaut, R. and G. Lemarquand, “Comparison of the coulombian and amperian current models for calculating the magnetic

- field produced by radially magnetized Arc-shaped permanent magnets,” *Progress In Electromagnetics Research*, Vol. 95, 309–327, 2009.
19. Tsai, M.-C., C.-C. Huang, and S.-Y. Shen, “Analysis method for motor characteristics with three-dimensional flux distribution,” *IEEE Transactions on Magnetics*, Vol. 40, No. 2, 443–450, March 2004.